(Received 18 July 2025, Accepted 1 September 2025, Scheduled 9 September 2025)

Compact CPW Fed Semi-Hexagonal Broadband CP Antenna for IoT Applications

Sasmita K. Nayak* and Sanjeev K. Mishra

RF Microwave Lab, Department of ETC, IIIT Bhubaneswar, Odisha, India

ABSTRACT: In this paper, a novel, compact, broadband circularly polarized (CP) semi-hexagonal monopole antenna is proposed. The antenna integrates a rectangular open loop and nonuniform asymmetric ground planes. The proposed design is fabricated on a 1.6 mm thick FR4 substrate with overall dimensions of $0.83\lambda_c \times 0.70\lambda_c \times 0.021\lambda_c$ at the center frequency $f_c = 3.935$ GHz. It achieves an impedance bandwidth of 4.51 GHz (1.68–6.19 GHz, 114.63%) and an axial ratio bandwidth of 2.6 GHz (2.3–4.9 GHz, 72.3%). The antenna offers realized gains of 1.4 dBi and 0.5 dBi, with corresponding efficiencies of 64% and 51% at 2.4 GHz and 3.5 GHz, respectively. It exhibits right-handed circular polarization (RHCP) across the ISM and WiMAX frequency bands. Furthermore, the antenna's performance is validated in a realistic environment using an Arduino-based wireless voltage monitoring system, demonstrating reliable data transmission with minimal loss. These results confirm the antenna's suitability for IoT applications requiring stable and efficient wireless communication.

1. INTRODUCTION

The Internet of Things (IoT) enables seamless connectivity among physical objects, machines, sensors, servers, and individuals, transforming healthcare, industrial automation, smart homes, and wearable technology through efficient data transmission and automation [1, 2]. To support IoT applications, reliable wireless communication is essential. Additionally, the Industrial, Scientific, and Medical (ISM) frequency bands facilitate low-power devices, including Wi-Fi, Bluetooth, Zigbee, Radio Frequency Identification (RFID), and for Near Field Communication (NFC) applications. However, interference from other radio frequency (RF) and microwave technologies necessitates advancements in RF front-end components, particularly antennas, to ensure reliable performance.

IoT antenna designs have been explored to meet the diverse connectivity demands of modern wireless communication systems. They include monopole antennas, slot antennas, multiple-input multiple-output (MIMO) antennas, and ultra-wideband (UWB) antennas, each offering unique advantages in terms of bandwidth, polarization, and diversity.

Certain state-of-the-art IoT antenna architectures utilizing slot techniques include a cavity-backed slot antenna operating at 900–925 MHz [3] and a pattern-reconfigurable antenna functioning at 2 GHz [4]. Similarly, MIMO techniques have been demonstrated in a quad-element super-wideband (SWB) MIMO antenna covering a frequency range from 3.1 GHz to 40 GHz [5] as well as in a compact 5G IoT MIMO system operating from 2 to 4 GHz [6]. Additionally, UWB antennas have gained attention due to their broad frequency coverage, with designs like a coplanar waveguide (CPW)-fed flexible UWB antenna spanning 3.2–30 GHz [6] and a compact UWB monopole antenna covering 3–9 GHz [7].

These IoT antennas provide wide impedance bandwidth but inefficient connectivity; most of them are linearly polarized, making them susceptible to polarization mismatch losses and multipath interference.

To enhance communication reliability, circularly polarized (CP) antennas are preferred, as they offer improved signal stability, polarization diversity, and better performance in dynamic environments. The advantages of CP antennas include reduced fading, enhanced link quality, and improved efficiency in multipath conditions, making them essential for modern wireless applications.

Several techniques have been explored to achieve circular polarization in antenna designs. They include asymmetric monopole shapes, where the radiator geometry is adjusted to create two orthogonal fields with a 90-degree phase difference [8, 9], slotting techniques that introduce slots within the radiator to generate CP radiation [10, 11], and ground plane modifications that enhance circular polarization characteristics [12, 13]. Additionally, parasitic elements have been used to improve axial ratio bandwidth (ARBW) [14, 15], and different feeding techniques, such as dual-feed or branched microstrip feeds, have been implemented to optimize CP performance [16, 17].

CPW-fed antennas have been developed with varying degrees of success in achieving broadband CP operation. Some notable designs include a CPW-fed antenna with an asymmetric ground plane operating from 4.35 to 8.15 GHz, achieving an axial ratio bandwidth (ARBW) of 60% [12], a planar antenna with an inverted L-shaped feed and a hook-shaped ground, obtaining CP with a 3 dB ARBW from 2.38 to 4.60 GHz (63.61%) [15],

* Corresponding author: Sasmita Kumari Nayak (c122009@iiit-bh.ac.in).

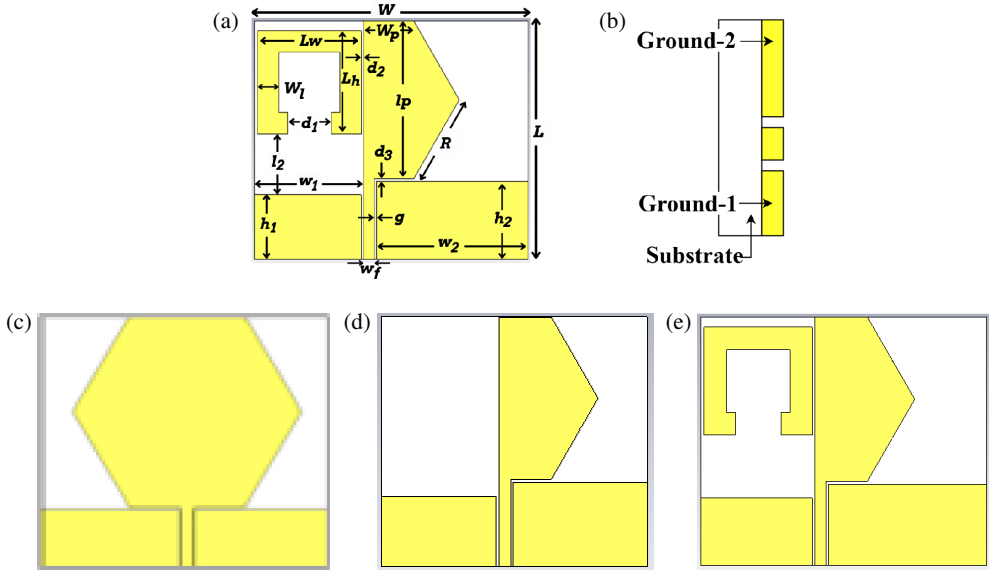

FIGURE 1. Evolution of the proposed semi-hexagonal antenna: (a) Geometry of proposed antenna, (b) Cross-sectional view, (c) Hex antenna, (d) Half Hex antenna, (e) Proposed semi-Hex antenna.

and a branched microstrip-fed antenna achieving an impedance bandwidth from 1.99 to 4.28 GHz and a CP bandwidth of 46.8% (2.13–3.43 GHz) [16]. Additionally, a monopole UWB patch antenna for on-body IoT applications has been reported, providing an impedance bandwidth of 124% (3.48–15 GHz) and an ARBW of 88.46% (3.48–9 GHz) [18].

However, many of these designs suffer from narrow ARBW relative to their impedance bandwidths and inconsistent CP performance across desired frequency bands. A few broadband CP antennas feature complex feed structures and intricate radiators that make them challenging to fabricate and embed into practical IoT devices [12, 16, 17, 19]. The existing CP antennas often fail to provide consistent CP features, which are not suitable for seamless integration to operate within Wi-Fi/WLAN bands. Therefore, further research is required to optimize IoT antenna designs for next-generation wireless communication systems, aiming for enhanced performance and reliability.

This paper presents a novel design that consists of a half-hexagonal radiating patch with a rectangular open loop and an asymmetric ground plane to achieve CP polarization features, operating in ISM and WiMAX bands. The proposed configuration is designed and optimized using Computer Simulation Technology (CST) model simulator, followed by fabrication and measurement. The antenna has also been tested in an IoT environment, and the obtained results confirm its suitability for portable wireless communication devices.

2. ANTENNA GEOMETRY AND DESIGN

2.1. Design Procedure

Figure 1 shows the evolution of the proposed semi-hexagonal CP antenna. The radiator is printed on a 1.6 mm thick FR4 substrate with relative permittivity $\varepsilon_r = 4.3$ and loss tangent $\tan\delta = 0.02$, and is fed through a 3 mm wide coplanar waveguide (CPW) line with an identical gap width of 'g'. The volumetric dimension of the proposed antenna is $W \times L \times h\,\text{mm}^3$, where W, L, and h represent the width, length, and height, respectively. The side length of the hexagonal patch is calculated using the equation [20].

$$R = \sqrt{\frac{\pi a_e^2}{3\sqrt{3}}} \tag{1}$$

where,

$$a_e = a \cdot \sqrt{1 + \frac{2h}{\pi a \varepsilon_r}\left[\ln\left(\frac{\pi a}{2h}\right) + 1.7726\right]} \tag{2}$$

$$a = \frac{F}{\sqrt{1 + \frac{2h}{\pi F \varepsilon_r}\left[\ln\left(\frac{\pi F}{2h}\right) + 1.7726\right]}} \tag{3}$$

$$F = \frac{8.791 \times 10^9}{f_r \varepsilon_r} \tag{4}$$

a_e is the effective radius of hexagon, a the actual radius of hexagon, and R the side length of hexagon.

Antenna-1 resonates over 2 GHz–4.9 GHz with the axial ratio near 40 dB within the band that exhibits linear polarization. Antenna-2 halves the hexagonal structure with an asymmetric ground plane which resonates over an impedance bandwidth from 2.5 to 6.5 GHz and ARBW from 4.0 to 5.95 GHz. In order to achieve CP at 2.4 GHz (ISM band) and 3.3–3.8 GHz [WiMAX], an additional open-loop stub is introduced in Antenna-3 that creates inductive and capacitive effects resulting in CP radiation in the lower band (2.3–4.9 GHz). The performance comparison is shown in Figure 2, and the optimized dimensions of the proposed antenna are listed in Table 1.

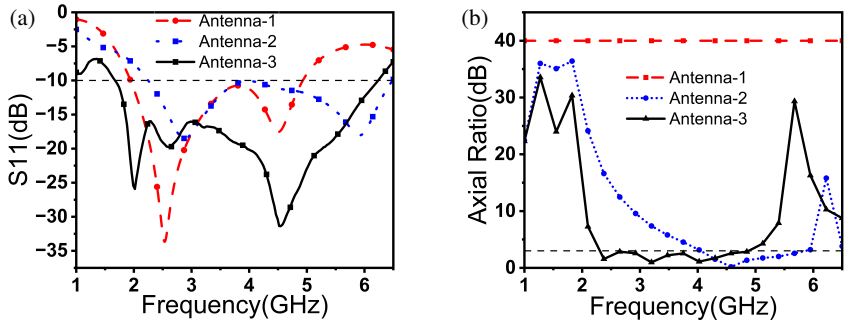

FIGURE 2. Comparison of all three antennas showing, (a) S_{11} and (b) Axial Ratio (AR) performance.

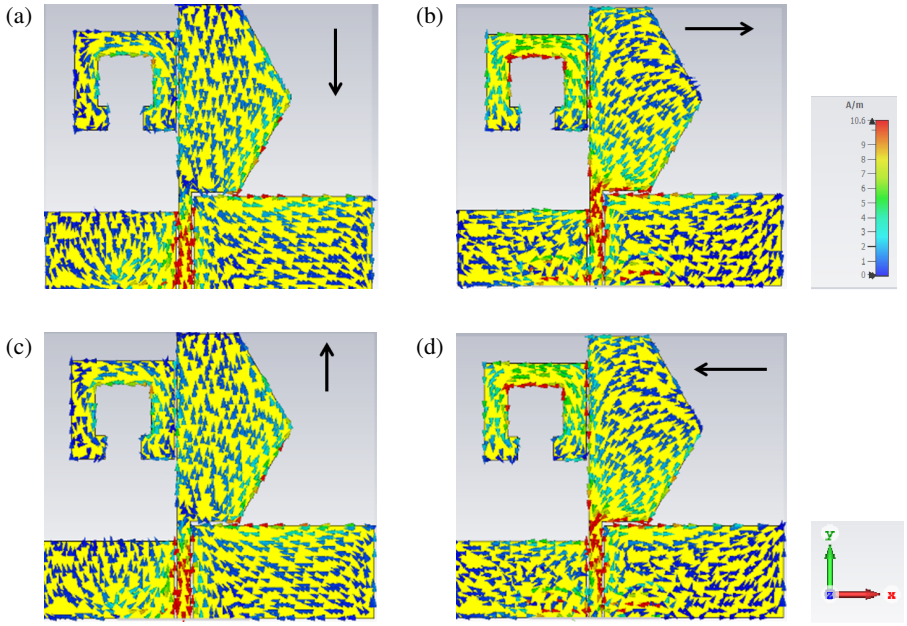

FIGURE 3. Surface current distribution at 2.4 GHz: (a) 0°, (b) 90°, (c) 180°, (d) 270°.

TABLE 1. Dimensions of proposed antenna (Unit: mm).

Parameter	Value	Parameter	Value
d_1	10	W	63.5
d_2	0.5	L	53.3
d_3	0.7	l_2	14
h_1	15	w_l	5
h_2	18.1	L_w	20
w_p	11.75	l_p	36.5
R	21	g	0.5
w_f	2.5	w_1	25
w_2	15.5	L_h	19

3. SIMULATION RESULTS

The return loss (S_{11}) and axial ratio (AR) of all proposed antennas are compared and shown in Figure 2. Antenna-1 is a conventional hexagon-shaped CPW-fed monopole antenna which resonates at 2.4 GHz. It exhibits linear polarization due to the opposing currents on the ground plane edge that creates out of phase waves to achieve CP characteristics. An asymmetric ground plane is introduced to create an imbalance in the surface current distribution in the antenna structure. This imbalance is crucial for generating the orthogonal modes necessary for CP. It is observed from Figure 2(b) that the AR of Antenna 1 is 40 dB because the horizontal components of the electric field get cancelled in the ground plane. Thus, the majority of vertical components result in a vertical polarization at 2.4 GHz. An asymmetric ground plane is used in Antenna 2 where the horizontal currents are confined to the right ground plane. Thus, the CP characteristic is observed from 4.3–5.9 GHz. In order to cover ISM (2.4–2.5 GHz) and WiMAX (3.3–3.8 GHz) bands, a rectangular open-loop stub is introduced at the side of the semi-hexagonal monopole antenna to provide capacitive coupling with the monopole, as shown in Figure 1(e). The loop provides reactive loading around 2.4 GHz, which modifies the current distribution and generates the lower band CP. Consequently, a broadband CP response with AR < 3 dB is achieved over 2.3–4.9 GHz.

In the proposed design, the right side of the extended ground plane is used to generate the right-hand circular polarization (RHCP) at higher frequency band. Similarly, at lower frequencies, the rectangular loop is introduced to achieve the RHCP. The validation is done by analysing the surface current distri-

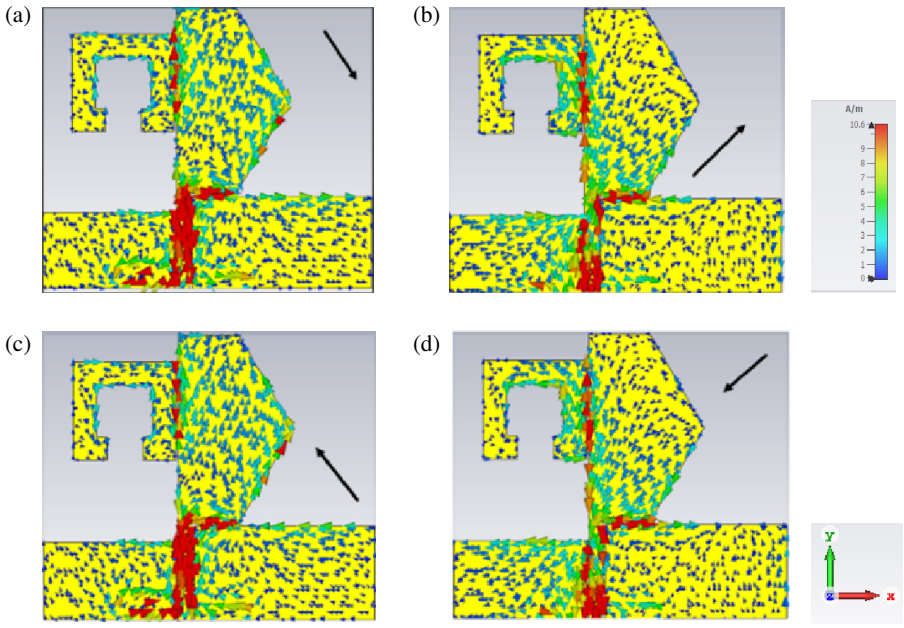

FIGURE 4. Surface current distribution at 3.6 GHz: (a) 0°, (b) 90°, (c) 180°, and (d) 270°.

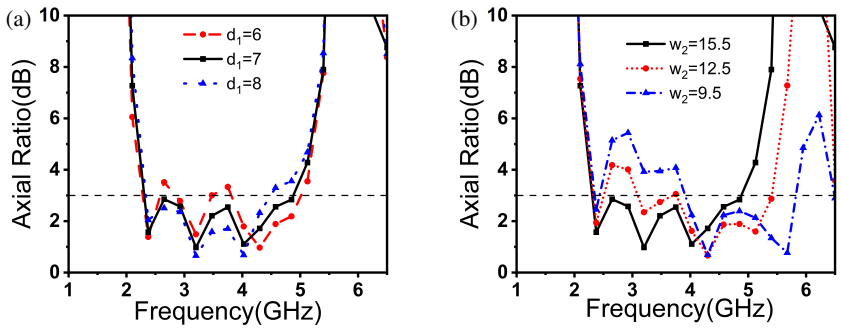

FIGURE 5. Simulated results of axial ratio (AR) with variation of (a) h_1 and (b) w_2.

bution shown in Figures 3 and 4. The surface current distributions in the proposed antenna are observed from the angles ranging from 0° to 270° which illustrate CP in the frequency bands. The resultant current in the antenna rotates anticlockwise with increasing time phase that exhibits RHCP radiation in the $+Z$ direction.

4. PARAMETRIC ANALYSIS

The parametric analysis of a semi-hexagonal CP antenna is carried out and discussed in this section. All the dimensions of the antenna affect the antenna characteristics, whereas the following dimensions, height and width, of the asymmetric ground plane, h_1 and w_1, control the impedance and axial ratio bandwidth. The height h_1 influences the current distribution of the ground plane and together with w_1, affects the effective path length, reflection phase on the ground plane, as well as the amplitude of the orthogonal components of the electric field. However, w_1 has minimal impact on the antenna's S_{11} and axial ratio (AR). In contrast, the height of the left side of the ground plane (h_1) significantly affects the antenna's axial ratio (AR). It is observed from Figure 5 that h_1 increases the AR in the lower band. When $h_1 = 13$ mm, AR is 3 dB obtained from 2.4–2.5 GHz, and when $h_1 = 17$ mm, the AR is obtained from 3.3–3.7 GHz. So, an optimal height of 15 mm is recommended.

At $h_1 = 15$ mm, the antenna is optimized to have a wider -10 dB impedance bandwidth and 3 dB AR bandwidth at 2.3–4.9 GHz. Another critical parameter is the length of Gnd-2, which is w_2 as it contributes to generating the horizontal components required for CP. The slanted side of the hexagonal monopole provides both vertical and horizontal components, making it necessary to generate additional horizontal components for effective CP creation. When the length of w_2 increases to 15.5 mm, a CP bandwidth AR below 3 dB is achieved, as illustrated in Figure 5(b). There are other parameters like position of loop, ratio of asymmetricity of ground plane, and feed position which contribute to getting a matching impedance as well as CP in the desired bands. Other crucial parameters to consider are length (L_h) and width (L_w), as shown in Figure 6(a), and loop openings (d_1) of the rectangular loop, as shown in Figure 6(b). L_h and L_w likely contribute to the generation of two orthogonal electric field components required for

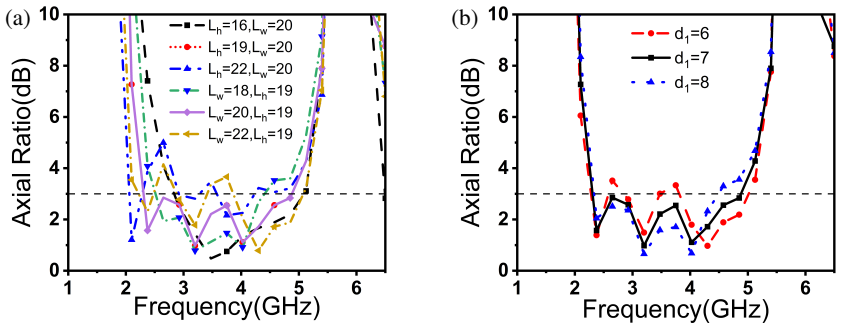

FIGURE 6. Simulated results of axial ratio (AR) with variation of (a) L_h, L_w and (b) d_1.

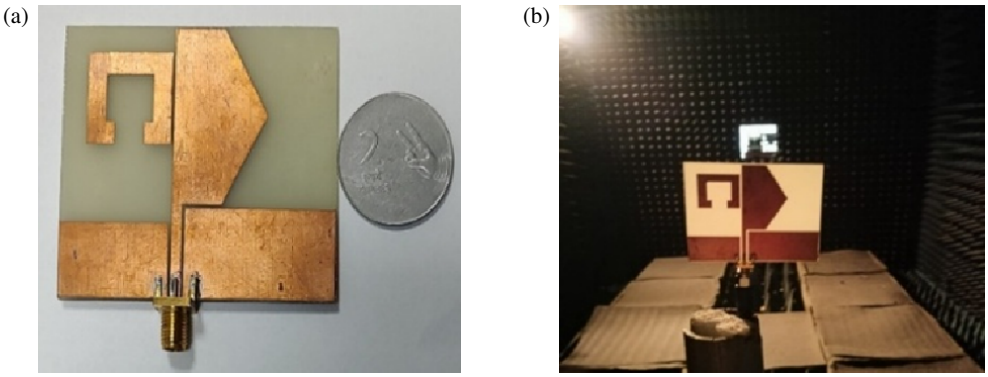

FIGURE 7. Measurement setup of the fabricated antenna showing (a) fabricated antenna prototype and (b) radiation pattern measurement setup.

circular polarization. By adjusting L_h and L_w, the phase difference between the orthogonal modes can be controlled. d_1 alters the effective electrical length of the loop, potentially shifting the antenna's resonance frequency. If the resonance is not aligned with the target frequency, the axial ratio may increase, leading to imperfect circular polarization. Proper tuning of d_1 is crucial for synchronizing the resonance of orthogonal modes, ensuring consistent circular polarization across the desired frequency range. As observed in Figure 6(a), variations in L_h cause the CP band to shift towards both higher and lower frequencies due to the capacitive effect, while the AR remains below 3 dB across the band. Decreasing L_w and d_1 impacts the AR because these dimensions contribute to the additional horizontal electric field. Therefore, the optimized values of L_h, L_w, and d_1 are 19 mm, 20 mm, and 7 mm respectively which are selected to maintain the AR ratio band within the desired frequency range. The lower band of the impedance bandwidth is influenced by these three parameters, while the higher band impedance matching and bandwidth remain unaffected.

5. MEASUREMENT RESULT

Figure 7(a) displays the fabricated antenna, while Figure 7(b) illustrates the antenna measurement setup inside an anechoic chamber. In this setup, a wideband horn antenna is employed as the transmitting antenna, and the fabricated antenna functions as the antenna under test (AUT). This configuration is utilized to assess the radiation characteristics in a controlled, reflection-free environment. Figure 8 illustrates the simulated antenna efficiency and gain across the frequency range of 1–6 GHz. The antenna achieves a peak efficiency of approximately 70% and maintains efficiency above 40% across a wide bandwidth. The realized gain reaches 1.4 dBi at 2.4 GHz and 0.5 dBi at 3.6 GHz, with corresponding total efficiencies of 64% and 51%, respectively, initiating stable performance suitable for broadband wireless applications. Figure 9 shows the simulated and measured results. The antenna achieves a wide 10 dB impedance bandwidth of 114.63% (1.68–6.19 GHz), with a 3-dB axial ratio bandwidth of 72.3% (2.3–4.9 GHz), confirming its wideband CP with good agreement between simulation and measurement. The antenna's performance aligns well with the design specifications, making it suitable for broadband communication applications in ISM and WiMAX bands.

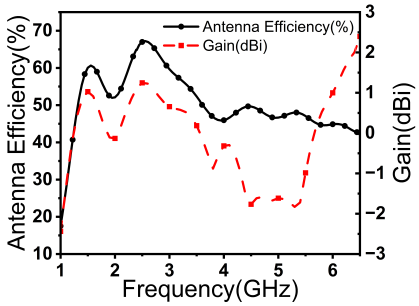

FIGURE 8. Gain and efficiency of the proposed antenna versus frequency.

Figures 10 & 11 show the simulated and measured normalized radiation patterns in the XZ ($\phi = 0°$) and YZ ($\phi = 90°$)

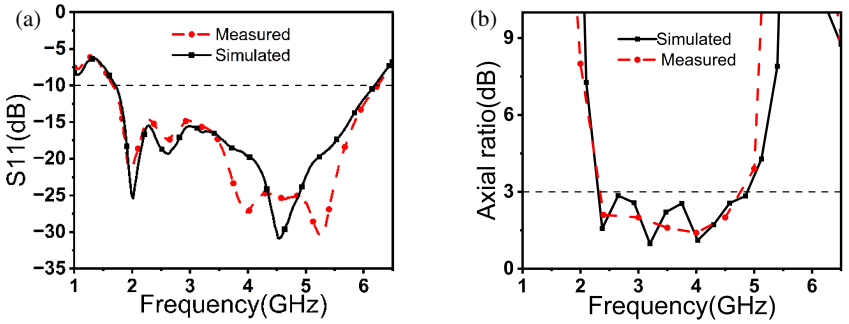

FIGURE 9. Simulated and measured performances of the proposed antenna with respect to frequency: (a) S_{11} and (b) axial ratio (AR).

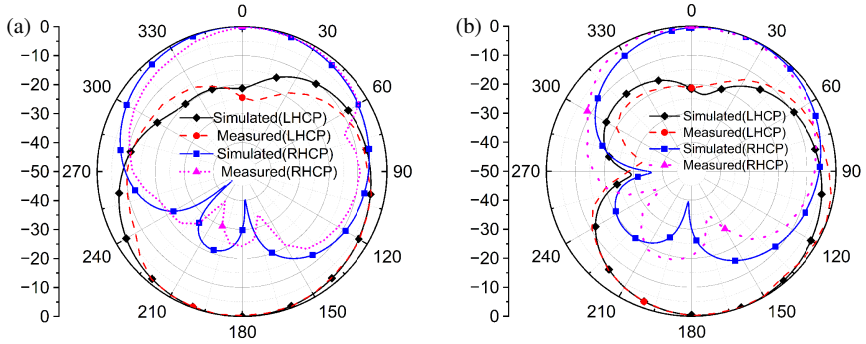

FIGURE 10. Simulated and measured radiation patterns of the proposed antenna at 2.4 GHz: (a) XZ plane and (b) YZ plane.

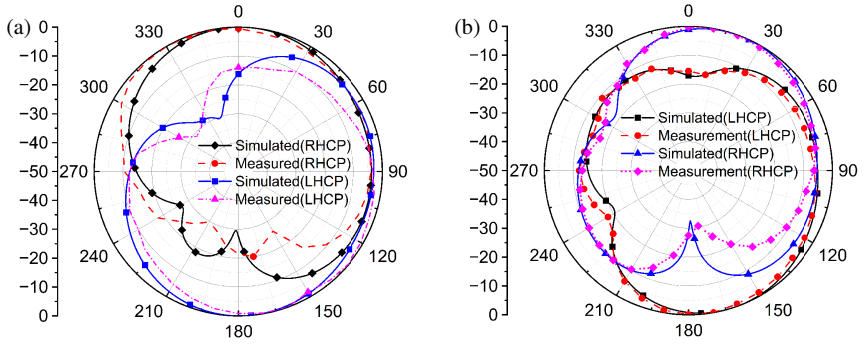

FIGURE 11. Simulated and measured radiation patterns of the proposed antenna at 3.6 GHz: (a) XZ plane and (b) YZ plane.

planes at 2.4 GHz and 3.6 GHz, respectively. In the case of 2.4 GHz, as shown in Figures 10(a) & (b), the RHCP gain of the antenna at 2.4 GHz is stronger than that of the LHCP gain by more than 20 dB in both planes, so it is an RHCP pattern in the $+Z$ direction.

Figure 11(a) demonstrates that the RHCP gain of the antenna at 3.6 GHz is significantly greater than the LHCP gain in both planes by more than 10 dB. So, the antenna shows RHCP pattern in the $+Z$ direction. The comparison with leading wideband CP and IoT application antennas is outlined in Table 2. Notably, the proposed antenna provides a broader impedance bandwidth than [12, 15, 21], all fabricated on an FR4 substrate. Additionally, the proposed CP antenna achieves enhanced ARBW compared to existing designs in [19, 21], which are enlisted in Table 2.

6. TESTING IN IOT ENVIRONMENTS

The proposed antenna is tested in a realistic IoT environment to assess its performance. Figure 12 illustrates the experimental setup, which comprises a wireless voltage monitoring system developed using an Arduino Uno as the transmitter and an Arduino Nano as the receiver, equipped with nRF24L01 transmitter and proposed antenna as the RF front-end of the receiver. A 47 kΩ potentiometer functions as a variable voltage source, with the Arduino Uno reading the analog voltage from pin A0 and transmitting it wirelessly. The transmitter continuously displays messages such as "Sending Voltage: 2.99" followed by "Data Sent Successfully," confirming successful data transmission. The receiver senses incoming data, displays "Received Voltage: 2.99" to indicate proper reception, and shows "Waiting . . ." when being ready for the next transmission.

TABLE 2. Comparison of proposed design with existing designs.

Ref	Substrate	Size (λ^3), f_c (GHz)	IBW (GHz), Percentage Bandwidth (%)	ARBW (GHz, %)	Peak Gain/ Radiation Effeciency (%)	IoT Applications and Testing
[6]	FR4	$1.18 \times 2.37 \times 0.031$, 3.0	2.4–3.8 (46.67)	–	5 dB/–	Yes/No
[7]	TECONIC	$0.235 \times 0.494 \times 0.0$, 4.92	3.0–9.0 (122)	–	−0.79 dB/–	Yes/No
[12]	FR4	$0.57 \times 0.57 \times 0.0116$, 6.25	3.0–9.0 (100)	4.35–8.15 (60)	4.5 dBi/–	No/No
[15]	FR4 (EPOXY)	$0.33 \times 0.33 \times 0.012$, 3.48	2.25–4.0 (56)	2.38–4.60 (63.61)	3 dBi/–	No/No
[18]	RO5880	$0.616 \times 0.462 \times 0.015$, 9.24	3.48–15.0 (124)	3.48–9 (88.46)	2.5 dBi/77	Yes/No
[19]	F4BM	$1.4 \times 1.47 \times 0.054$, 5.5	4.88–6.62 (30.6)	5.0–6.0 (22.2)	11.2 dBi/84	No/No
[21]	FR4	$0.5 \times 0.55 \times 0.016$, 3.0	1.48–3.95 (95)	2.05–3.95 (63.3)	0.5 dBi/–	No/No
[22]	FR4	$0.78 \times 0.78 \times 0.016$, 4.88	1.66–8.10 (131.97)	2.0–6.5 (105.88)	5.2 dBi/–	No/No
[23]	Roger 4350B	$1.93 \times 1.93 \times 0.178$, 5.85	5.6–6.1 (8.55)	5.6–6.1 (8.55)	−20 dBi/19.3	Yes/No
[24]	Jeans	$1.44 \times 0.46 \times 0.0512$, 5.41	4.76–6.08 (24.40)	–	10.59 dBi/85	Yes/No
[25]	FR4	$1 \times 1.85 \times 0.024$, 2.83	Multi-band	–	5.20 dBi/–	Yes/Yes
[26]	RO3003	$0.328 \times 0.352 \times 0.0122$, 2.4	2.38–2.44 (3.8), 5.675–5.975 (5.2)	–	–	Yes/Yes
Proposed	FR4	$0.83 \times 0.70 \times 0.021$, 3.935	1.68–6.19 (114.63)	2.3–4.9 (72.3)	2.5 dBi/70	Yes/Yes

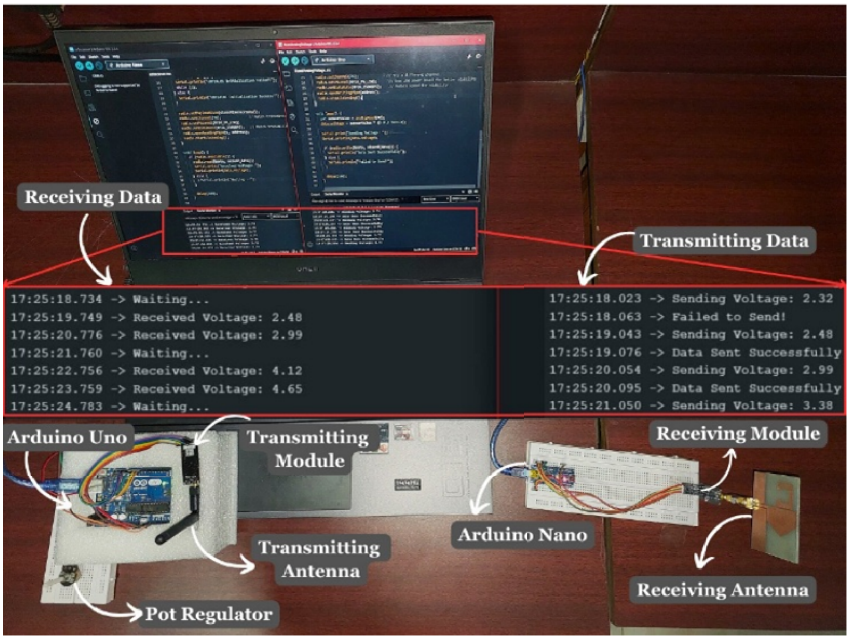

FIGURE 12. Experimental setup for IoT applications.

7. CONCLUSION

A low-profile, compact broadband semi-hexagonal monopole CP antenna is proposed and investigated. The proposed antenna demonstrates a wide circular polarization performance, achieving a measured 10-dB impedance bandwidth of 114.6% (1.68–6.19 GHz) and a broad 3-dB axial ratio bandwidth of 72.3% (2.3–4.9 GHz). The proposed antenna is an attractive candidate for ISM, WiMAX, and other broadband communication systems. For IoT applications, the antenna is tested in a realistic environment using an Arduino-based transmitter and receiver system, demonstrating stable data transmission and minimal packet loss. The custom-fabricated antenna significantly improved performance compared to a standard nRF24L01 antenna, ensuring reliable wireless voltage monitoring with excellent stability. This makes the proposed antenna a promising solution for IoT applications.

REFERENCES

[1] Shafique, K., B. A. Khawaja, F. Sabir, S. Qazi, and M. Mustaqim, "Internet of things (IoT) for next-generation smart systems: A review of current challenges, future trends and prospects

for emerging 5G-IoT scenarios," *IEEE Access*, Vol. 8, 23 022–23 040, 2020.

[2] Sahu, N. K., N. C. Naik, M. C. Tripathy, and S. K. Mishra, "A review of the advancement of metasurfaces in wearable antenna design for off-body communications," *Progress In Electromagnetics Research B*, Vol. 104, 91–108, 2024.

[3] Oh, J.-I., H.-W. Jo, K.-S. Kim, H. Cho, and J.-W. Yu, "A compact cavity-backed slot antenna using dual mode for IoT applications," *IEEE Antennas and Wireless Propagation Letters*, Vol. 20, No. 3, 317–321, 2021.

[4] Shah, S. S., S. Koziel, S. Bashir, E. Bernhardsson, A. Salim, and S. I. H. Shah, "Pattern reconfigurable quasi Yagi antenna with Origami inspired magic spiral cubes for dynamic indoor IoT applications," *Scientific Reports*, Vol. 15, No. 1, 10023, 2025.

[5] Kumar, P., S. Urooj, and A. Malibari, "Design and implementation of quad-element super-wideband MIMO antenna for IoT applications," *IEEE Access*, Vol. 8, 226 697–226 704, 2020.

[6] Chattha, H. T., M. K. Ishfaq, B. A. Khawaja, A. Sharif, and N. Sheriff, "Compact multiport MIMO antenna system for 5G IoT and cellular handheld applications," *IEEE Antennas and Wireless Propagation Letters*, Vol. 20, No. 11, 2136–2140, 2021.

[7] Bekasiewicz, A. and S. Koziel, "Compact UWB monopole antenna for internet of things applications," *Electronics Letters*, Vol. 52, No. 7, 492–494, 2016.

[8] Behera, B. R. and S. K. Mishra, "Investigation of a high-gain and broadband circularly polarized monopole antenna for RF energy-harvesting application," *International Journal of Microwave and Wireless Technologies*, Vol. 15, No. 5, 781–792, 2023.

[9] Tiwari, R. N., P. Singh, and B. K. Kanaujia, "Asymmetric U-shaped printed monopole antenna embedded with T-shaped strip for bluetooth, WLAN/WiMAX applications," *Wireless Networks*, Vol. 26, No. 1, 51–61, 2020.

[10] Zhou, C. F. and S. W. Cheung, "A wideband CP crossed slot antenna using 1-λ resonant mode with single feeding," *IEEE Transactions on Antennas and Propagation*, Vol. 65, No. 8, 4268–4273, 2017.

[11] Verma, M. K., B. K. Kanaujia, J. P. Saini, and P. Singh, "A compact multi-slots loaded gap coupled CP antenna with DGS for WLAN/WiMAX applications," *International Journal of RF and Microwave Computer-Aided Engineering*, Vol. 30, No. 12, e22431, 2020.

[12] Felegari, N., S. Zafari, N. Malekpour, and H. R. Hassani, "A CPW-fed compact square slot antenna with wideband circularly polarized for C-band application," *Microwave and Optical Technology Letters*, Vol. 63, No. 3, 862–868, 2021.

[13] Ullah, U. and S. Koziel, "A geometrically simple compact wideband circularly polarized antenna," *IEEE Antennas and Wireless Propagation Letters*, Vol. 18, No. 6, 1179–1183, 2019.

[14] Alsariera, H., Z. Zakaria, and A. A. M. Isa, "A broadband P-shaped circularly polarized monopole antenna with a single parasitic strip," *IEEE Antennas and Wireless Propagation Letters*, Vol. 18, No. 10, 2194–2198, 2019.

[15] Midya, M., S. Bhattacharjee, and M. Mitra, "Broadband circularly polarized planar monopole antenna with G-shaped parasitic strip," *IEEE Antennas and Wireless Propagation Letters*, Vol. 18, No. 4, 581–585, 2019.

[16] Samsuzzaman, M., M. T. Islam, and M. J. Singh, "A compact printed monopole antenna with wideband circular polarization," *IEEE Access*, Vol. 6, 54 713–54 725, 2018.

[17] Wu, Q.-S., X. Zhang, and L. Zhu, "A feeding technique for wideband CP patch antenna based on 90° phase difference between tapped line and parallel coupled line," *IEEE Antennas and Wireless Propagation Letters*, Vol. 18, No. 7, 1468–1471, 2019.

[18] Pandey, U., P. Singh, R. Singh, N. P. Gupta, S. K. Arora, and E. Nizeyimana, "Miniaturized ultrawideband microstrip antenna for IoT-based wireless body area network applications," *Wireless Communications and Mobile Computing*, Vol. 2023, No. 1, 3950769, 2023.

[19] Xu, Y., H. Hu, B. Chen, M. Chen, J. Tian, and S. Lei, "Broadband high-gain circularly polarized antenna for conformal applications," *IEEE Antennas and Wireless Propagation Letters*, Vol. 22, No. 8, 2032–2036, 2023.

[20] Balanis, C. A., *Antenna Theory: Analysis and Design*, 4th ed., John Wiley & Sons, 2016.

[21] Ding, K., Y.-X. Guo, and C. Gao, "CPW-fed wideband circularly polarized printed monopole antenna with open loop and asymmetric ground plane," *IEEE Antennas and Wireless Propagation Letters*, Vol. 16, 833–836, 2016.

[22] Gunjal, A. and U. Kshirsagar, "Broadband asymmetrically fed circularly polarized slot antenna for mid-band 5G smartphone applications," *Progress In Electromagnetics Research C*, Vol. 115, 233–244, 2021.

[23] Ma, L., J. Lu, C. Gu, and J. Mao, "A wideband dual-circularly polarized, simultaneous transmit and receive (STAR) antenna array for integrated sensing and communication in IoT," *IEEE Internet of Things Journal*, Vol. 10, No. 7, 6367–6376, 2023.

[24] Dey, A. B., S. Kumar, W. Arif, and J. Anguera, "Elastomeric textile substrates to design a compact, low-profile AMC-based antenna for medical and IoT applications," *IEEE Internet of Things Journal*, Vol. 10, No. 6, 4952–4969, 2023.

[25] Jha, K. R., B. Bukhari, C. Singh, G. Mishra, and S. K. Sharma, "Compact planar multistandard MIMO antenna for IoT applications," *IEEE Transactions on Antennas and Propagation*, Vol. 66, No. 7, 3327–3336, 2018.

[26] Musa, U., S. M. Shah, H. A. Majid, I. A. Mahadi, M. K. A. Rahim, M. S. Yahya, and Z. Z. Abidin, "Design and implementation of active antennas for IoT-based healthcare monitoring system," *IEEE Access*, Vol. 12, 48 453–48 471, 2024.